Electroweak corrections to dilepton production via photon fusion at LHC

V. A. Zykunov, JINR

Moscow, 24–30 August, 2023
21st Lomonosov Conference
on Elementary Particle Physics

Introduction

Despite the fact that the Standard Model (SM) keeps for oneself the status of consistent and experimentally confirmed theory, the search of New Physics (NP) manifestations is continued:

- ⋆ **the supersymmetry**,
- ⋆ **M-theory**,
- ⋆ **DM-particles**,
- ⋆ **axions**,
- ⋆ **feebly interacting particles**,
- ⋆ **extra** spatial dimensions,
- ⋆ **extra** neutral gauge bosons, etc.

One of powerful tool in the modern experiments at LHC is the investigation of **Drell–Yan dilepton production**

$$pp \to \gamma, Z \to l^+ l^- X \qquad (1)$$

at **large invariant mass** of lepton pair: $M \geq 1$ TeV.

Drell-Yan process (1970, BNL)

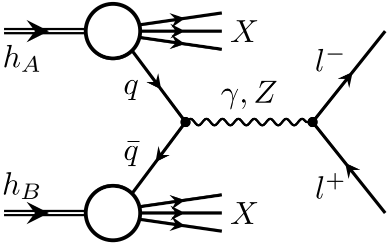

Figure 1: Drell-Yan process with neutral current

★ $\sqrt{S}$ is total energy in c.m.s. of hadrons

★ M is dilepton l^+l^- invariant mass ($l = e, \mu$)

★ y is dilepton rapidity

Current experimental situation at CMS LHC

★ The measured Drell–Yan cross sections and forward-backward asymmetries are consistent with the SM predictions at

$$\sqrt{S} = 7\text{–}8 \text{ TeV } (19.7 \text{ fb}^{-1}) \text{ for } M \leq 2 \text{ TeV},$$

$$\sqrt{S} = 13 \text{ TeV } (85 \text{ fb}^{-1}) \text{ for } M \leq 3 \text{ TeV}$$

- ★ differential cross section $\frac{d\sigma}{dM}$,
- ★ double-differential cross section $\frac{d^2\sigma}{dMdy}$,
- ★ forward-backward asymmetry A_{FB}.

★ NNLO RCs are taken into account by using of **FEWZ**,

★ NNLO PDFs are **CT10 NNLO** and **NNPDF2.1**.

Some modern codes for NLO and NNLO RC for DY process at hadronic colliders (in the ABC order)

- ★ DYNNLO (S. Catani, L. Cieri, G. Ferrera et al.)
- ★ FEWZ (R. Gavin, Y. Li, F. Petriello, S. Quackenbush)
- ★ HORACE (C.Carloni Calame, G.Montagna, et al.)
- ★ MC@NLO (S. Frixione, F. Stoeckli, P. Torrielli et al.)
- ★ PHOTOS (N. Davidson, T. Przedzinski, Z. Was et al.)
- ★ POWHEG (L. Barze, G. Montagna, P. Nason et al.)
- ★ RADY (S. Dittmaier, A. Huss, C. Schwinn et al.)
- ★ READY (V. Zykunov, RDMS CMS)
- ★ SANC (Dubna: A. Andonov, A. Arbuzov, D. Bardin et al.)
- ★ WINHAC (W. Placzek, S. Jadach, M.W. Krasny et al.)
- ★ WZGRAD (U. Baur, W. Hollik, D. Wackeroth et al.)

Code READY and a set of prescriptions

In the following the scale of radiative corrections and their effect on the observables of Drell–Yan processes will be discussed using FORTRAN program **READY**: (**R**adiative corr**E**ctions to l**A**rge invariant mass **D**rell–**Y**an process).

We used the following set of prescriptions:

- ★ standard PDG set of SM input electroweak parameters,
- ★ "effective" quark masses ($\Delta\alpha^{(5)}_{had}(m_Z^2) = 0.0276$),
- ★ 5 active flavors of quarks in proton,
- ★ CTEQ, CT10, and MHHT14 sets of PDFs,
- ★ choice for PDFs: $Q = M_{sc} = M$.

CMS detector setup

We impose the experimental restriction conditions

★ on the detected lepton angle $-\zeta^* \leq \cos\theta \leq \zeta^*$ (or on the rapidity $|y(l)| \leq y(l)^*$); for CMS detector the cut values of ζ^* (or $y(l)^*$) are determined as

$$\zeta^* \approx 0.986614 \quad (\text{or} \quad y(l)^* = 2.5),$$

★ the second standard CMS restriction $p_T(l) \geq 20$ GeV,

★ the "bare" setup for muon identification requirements (no smearing, no recombination of muon and photon/gluon).

Mathematical Content

At the edges of kinematical region (extra large $\sqrt{S}$, M) the important task is make the RC procedure both accurate and fast. For the latter it is desirable to obtain **the set of compact formulas** for the EWK and QCD RCs.

Leading effect of **Weak RCs** in the region of large M is described by the Sudakov Logarithms (**SL; V. Sudakov, 1956**):

$$\log \frac{m_B^2}{|r|} \quad (B = Z, W; \quad r = s, t, u). \tag{2}$$

Collinear Logarithms (**CL**) play leading role in description of **QED RCs and QCD RCs**:

$$\log \frac{m_f^2}{|r|} \quad (f = e, \mu, q; \quad r = s, t, u). \tag{3}$$

Notations, invariants, coupling constants

The standard set of **Mandelstam invariants** for the partonic elastic scattering:

$$s = (p_1 + p_2)^2, \quad t = (p_1 - k_1)^2, \quad u = (k_1 - p_2)^2. \tag{4}$$

The propagator for j-boson depends on its mass and width:

$$D^{js} = \frac{1}{s - m_j^2 + i m_j \Gamma_j}. \tag{5}$$

Suitable combinations of coupling constants are:

$$\lambda_f{}_+^{i,j} = v_f^i v_f^j + a_f^i a_f^j, \quad \lambda_f{}_-^{i,j} = v_f^i a_f^j + a_f^i v_f^j, \tag{6}$$

$$v_f^\gamma = -Q_f, \quad a_f^\gamma = 0, \quad v_f^Z = \frac{I_f^3 - 2 s_W^2 Q_f}{2 s_W c_W}, \quad a_f^Z = \frac{I_f^3}{2 s_W c_W}.$$

Main features of EWK and QCD RCs calculation

The notations, the Feynman rules and renomalization detailes are inspired by review of **M. Böhm, H. Spiesberger, and W. Hollik, 1986**:

- ⋆ **the t'Hooft–Feynman gauge**,
- ⋆ **on-mass renormalization scheme** ($\alpha, \alpha_s, m_W, m_Z, m_H$ and the fermion masses as independent parameters),
- ⋆ **ultrarelativistic approximation**.

QCD result can be obtained from QED case by substitution:

$$Q_q^2\alpha \to \sum_{a=1}^{N^2-1} t^a t^a \alpha_s = \frac{N^2-1}{2N} I\alpha_s \to \frac{4}{3}\alpha_s, \quad (7)$$

here $2t^a$ – Gell-Man matrices, and $N = 3$.

Two mechanisms: DY and $\gamma\gamma$-fusion

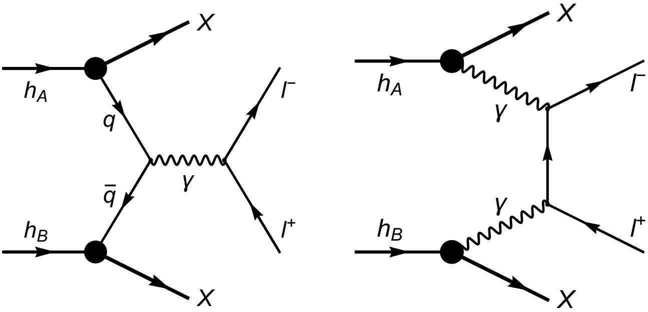

Figure 2: Dilepton production in hadron collisions: left – the Drell–Yan process with virtual photon, right – the photon-photon fusion.

$\gamma\gamma$-fusion Born: diagrams and cross sections

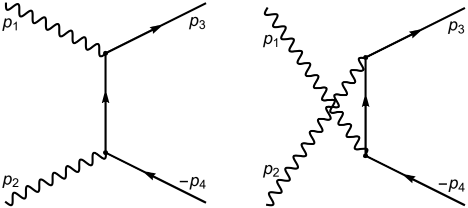

Figure 3: Feynman diagrams of $\gamma\gamma \to l^- l^+$ process at Born level.

Parton level:

$$d\sigma_0^{\gamma\gamma} = \frac{2\pi\alpha^2}{s^2}\frac{t^2+u^2}{tu}dt. \qquad (8)$$

Hadron level ($\mathcal{C} = \cos\theta$):

$$\frac{d^3\sigma_0^h}{dMdyd\mathcal{C}} = 8\pi\alpha^2 f_\gamma^A(x_1) f_\gamma^B(x_2)\frac{t^2+u^2}{SM^5(1-\mathcal{C}^2)}\Theta. \qquad (9)$$

DY vs $\gamma\gamma$: diff. cross section $d\sigma/dM$

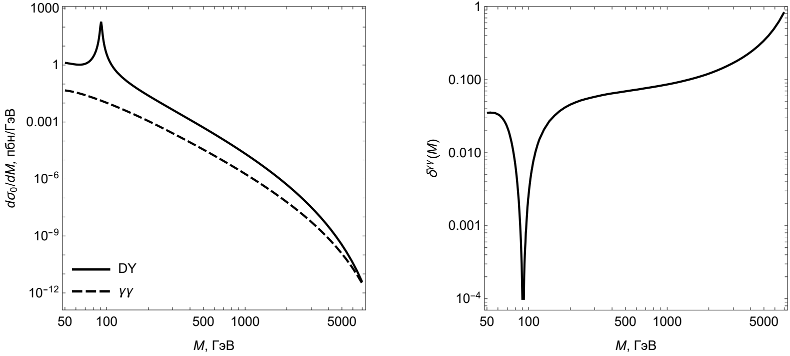

Figure 4: Left – differential Born cross section via M, right – the relative correction $\delta^{\gamma\gamma}(M)$ via M:

$$\delta^{\gamma\gamma}(M) = \frac{d\sigma_0^{\gamma\gamma}/dM}{d\sigma_0^{\mathrm{DY}}/dM}. \tag{10}$$

DY vs $\gamma\gamma$: double diff. cross section $d^2\sigma/dMdy$

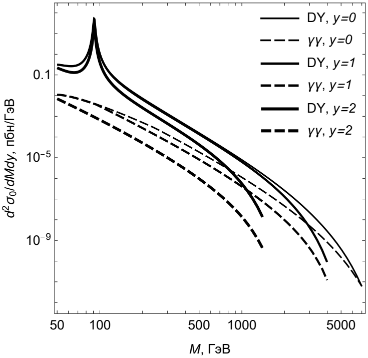

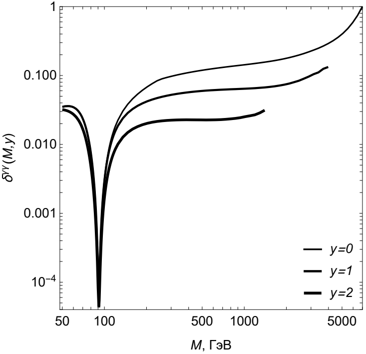

Figure 5: Left – double differential cross sections via M at different y. right – the relative corrections $\delta^{\gamma\gamma}(M, y)$ via M at different y.

Virtual diagrams: γ and Z

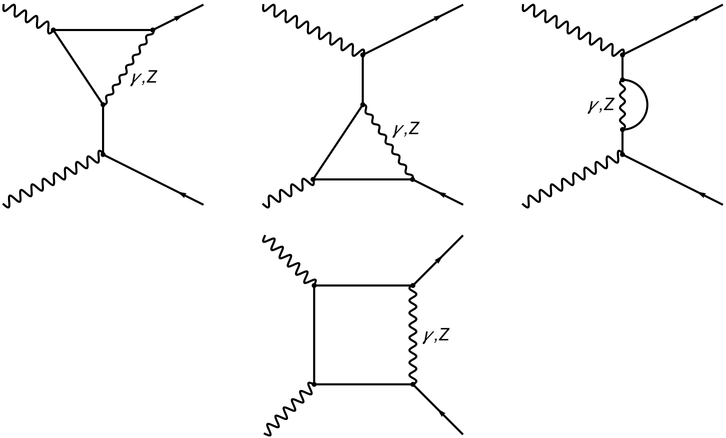

Figure 6: Half of Feynman diagrams set for $\gamma\gamma \to l^- l^+$ process with additional virtual γ and Z-boson: vertices, electron self energies, boxes. The rest diagrams are obtained by $p_1 \leftrightarrow p_2$.

Virtual diagrams: W

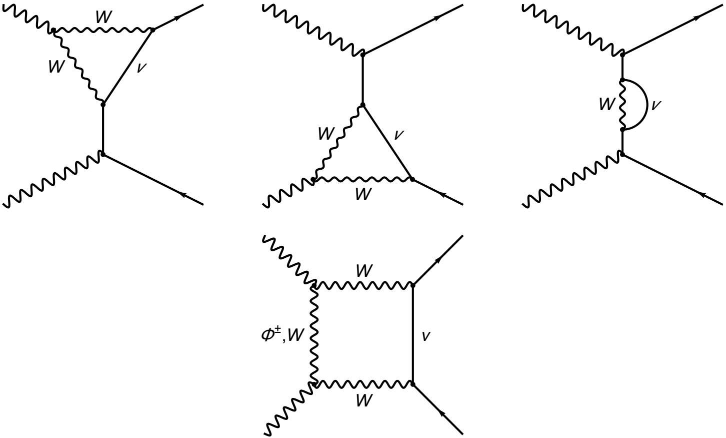

Figure 7: Half of Feynman diagrams set for $\gamma\gamma \to l^- l^+$ process with additional virtual W-boson: vertices, electron self energies, boxes. The rest diagrams are obtained by $p_1 \leftrightarrow p_2$.

Bremshtrahlung diagrams

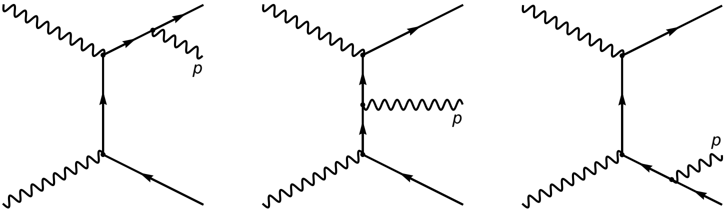

Figure 8: Half of Feynman diagrams set for $\gamma\gamma \to l^- l^+ \gamma$ process. The rest diagrams are obtained by $p_1 \leftrightarrow p_2$.

Virtual + soft contribution

The virtual and soft contributions are factorized before Born cross section **(M. Böhm and T. Sack, 1986)**:

$$\delta_{\rm QED} = \frac{\alpha}{\pi}\Big(\log\frac{4\omega^2}{s}(L-1) + \frac{\pi^2}{3} - \frac{3}{2} + \frac{tu}{t^2+u^2}[f(t,u)+f(u,t)]\Big),$$

where the function

$$f(t,u) = \frac{s^2+t^2}{2tu}L_{st}^2 - \frac{3u}{2t}LL_{st} - L_{st}.$$

is entering in the cross section symmetrically (with $t \leftrightarrow u$), and the **collinear "big" log** and **angle log** look like:

$$L = \log\frac{s}{m^2}, \quad L_{st} = \log\frac{s}{-t}. \qquad (11)$$

Weak contributions: Z and W

The **weak corrections** are factorized too:

$$\delta_Z = -\frac{\alpha}{\pi}(v_Z^2 + a_Z^2)\frac{tu}{t^2+u^2}\Big[G_Z(t,u) + G_Z(u,t)\Big],$$
$$\delta_W = -\frac{\alpha}{\pi}\frac{1}{4s_W^2}\frac{tu}{t^2+u^2}\Big[G_W(t,u) + G_W(u,t)\Big].$$

Assuming the **HE asymptotic** $\sqrt{s} \gg m_Z$ we get:

$$G_Z^{\mathrm{HE}}(t,u) = \frac{t^3 L_{st}^2}{2u^3} + \frac{tL_{tZ}}{2u}(L_{sZ} + L_{st} - 1) - \frac{tL_{sZ}}{u} - \frac{t^2 L_{st}}{u^2} + \frac{t(27-2\pi^2)}{12u},$$

$$G_W^{\mathrm{HE}}(t,u) = \frac{t^2}{su}(\pi^2 - L_{sW}^2) + \frac{t}{u}\left(\frac{\pi^2}{3} + L_{tW}^2\right) - \frac{3u}{2t}L_{tW} - L_{st} + \frac{5u}{4t},$$

where **Sudakov logs** look like:

$$L_{tB} = \log\frac{-t}{m_B^2}, \quad L_{sB} = \log\frac{s}{m_B^2}; \quad B = Z, W.$$

Independance of unphysical parameter ω

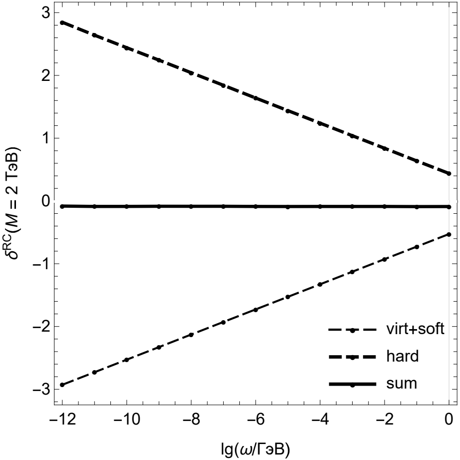

Figure 9: The relative corrections $\delta^{\rm RC}$ to differential cross section $\frac{d\sigma}{dM}$ (virtual and soft, hard, their sum) via ω (M=2 TeV).

Relative correction definition:

$$\delta^{\rm RC}(M) = \frac{d\sigma^{\gamma\gamma}_{\rm RC}/dM}{d\sigma^{\gamma\gamma}_0/dM}.$$

ElectoMagnetic corrections to diff. cross section $d\sigma/dM$

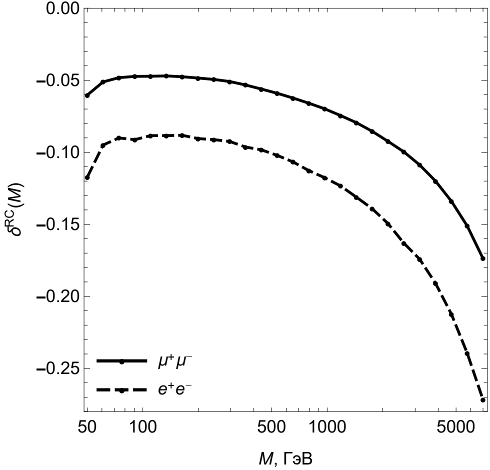

Figure 10: Total relative electromagnetic corrections $\delta^{\mathrm{RC}}(M)$ via M.

ElectoMagnetic corrections to double diff. cross section

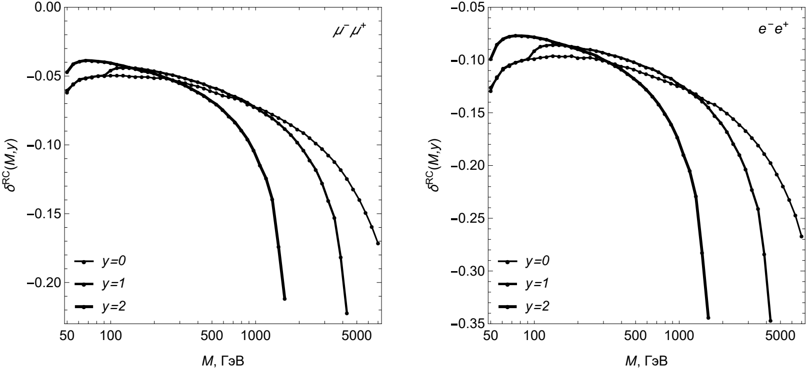

Figure 11: Total relative electromagnetic corrections $\delta^{\mathrm{RC}}(M, y)$ to $\frac{d^2\sigma_0}{dMdy}$ via M at different y.

ElectoWeak corrections to $\frac{d\sigma_0}{dM}$ and $\frac{d^2\sigma_0}{dMdy}$

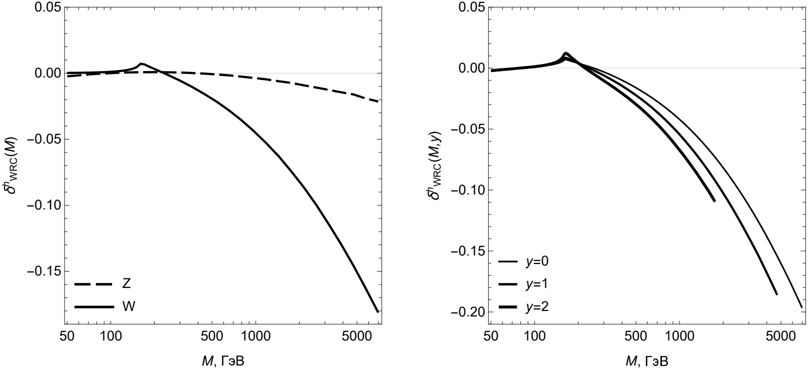

Figure 12: Left (right) – relative electroweak corrections to differential cross section (to double differential cross section at different y) via M.

Total cross sections: standard CMS bins

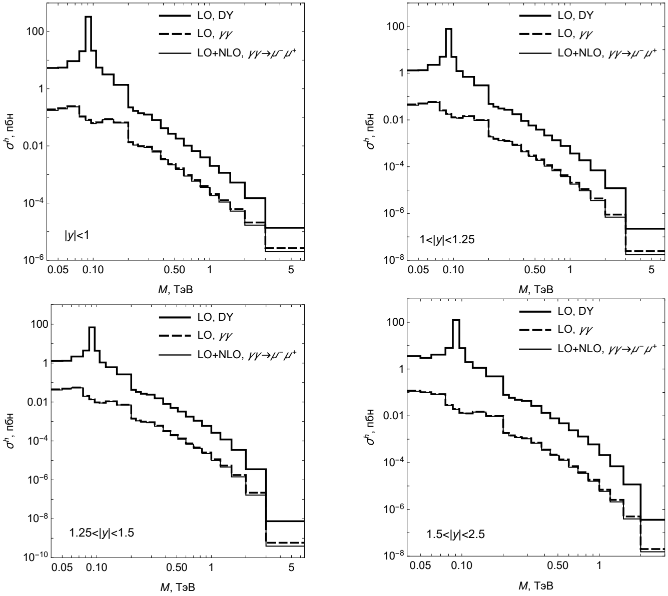

Forward-backward asymmetry

Forward-backward asymmetry $A_{\rm FB}$ is important observable in dilepton production **with a dual nature – electroweak and kinematical**:

$$A_{\rm FB} = \frac{\sigma^h_{\rm F} - \sigma^h_{\rm B}}{\sigma^h_{\rm F} + \sigma^h_{\rm B}}, \qquad (12)$$

where according **J. Collins & D. Soper (1977)**:

$\sigma^h_{\rm F}$ is "forward" cross section ($\cos\theta^* > 0$),

$\sigma^h_{\rm B}$ is "backward" cross section ($\cos\theta^* < 0$).

In the Collins–Soper system $\cos\theta^*$ looks like:

$$\cos\theta^* = {\rm sgn}[x_2(t+u_1) - x_1(t_1+u)]\frac{tt_1 - uu_1}{M\sqrt{s(u+t_1)(u_1+t)}}.$$

Forward, Backward (and Experimental) borders

For the case of nonradiative kinematics the $\cos\theta^*$ has especially simple view:

$$\cos\theta^* = \mathrm{sgn}[x_1 - x_2]\frac{u-t}{s} = \mathrm{sgn}\left[e^y - e^{-y}\right]\frac{(1+\mathcal{C})e^{-y} - (1-\mathcal{C})e^y}{(1+\mathcal{C})e^{-y} + (1-\mathcal{C})e^y}.$$

Solving $\cos\theta^* = 0$ we get **two conditions** for border dividing the regions of σ_{F}^h and σ_{B}^h:

$$y = 0, \quad \mathcal{C} \equiv \cos\theta = \mathrm{th}\, y.$$

The CMS experimental condition $|\cos\theta| < \zeta^*$ is trivial but the second one $|\cos\alpha| < \zeta^*$ is rather sophisticated:

$$\cos\left(\arccos\frac{\cos\theta - \mathrm{th}\, y}{r} + \arcsin\frac{\sin\theta\, \mathrm{th}\, y}{r}\right) = \pm\xi^*,$$

where

$$r = \sqrt{1 - 2\cos\theta\, \mathrm{th}\, y + \mathrm{th}^2\, y}.$$

Forward, Backward (and Experimental) regions

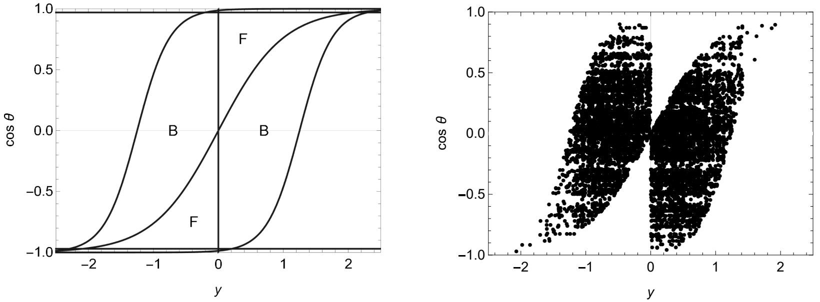

Figure 14: Left – Forward, Backward and CMS regions in y and $\cos\theta$ variables (**borders are**: $y = 0$, $\cos\theta = \operatorname{th} y$, $\cos\theta = \pm\zeta^*$, and $\cos\alpha = \pm\zeta^*$, where $\zeta^* \approx 0.9866$),
right – the points sampled by Monte-Carlo generator of VEGAS **for Backward CMS region**.

Interplay of DY and $\gamma\gamma$ for A_{FB}: numerical effect

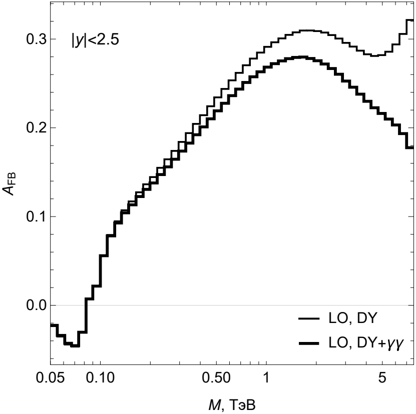

Figure 15: The Born forward-backward asymmetry via M at CMS LHC setup: for **Drell–Yan mechanism** – thin line, for **both mechanisms** (DY and $\gamma\gamma$-fusion) – thick line.

Interplay of DY and $\gamma\gamma$ for $A_{\rm FB}$: explanation

As the Born process $\gamma\gamma$-fusion has **pure electromagnetic nature**, then

$$A_{\rm FB}^{\gamma\gamma} = 0.$$

Therefore the F- an B- cross section are equal:

$$\sigma_{\rm F}^{\gamma\gamma} = \sigma_{\rm B}^{\gamma\gamma} = \Delta.$$

The $\gamma\gamma$-fusion cross section has the scale comparable with DY one **at large M region**. Expanding the net asymmetry (DY+$\gamma\gamma$) in series on Δ we get:

$$A_{\rm FB}^{\rm DY+\gamma\gamma} \approx A_{\rm FB}^{\rm DY}\left(1 - \frac{2\Delta}{\sigma_{\rm F+B}^{\rm DY}}\right).$$

This effect (the decreasing of net asymmetry at large M) is well seen in Fig. 15 starting with $M{\sim}300$ GeV.

$A_{\rm FB}$ for Run3 of CMS LHC: $\mu^+\mu^-$, DY

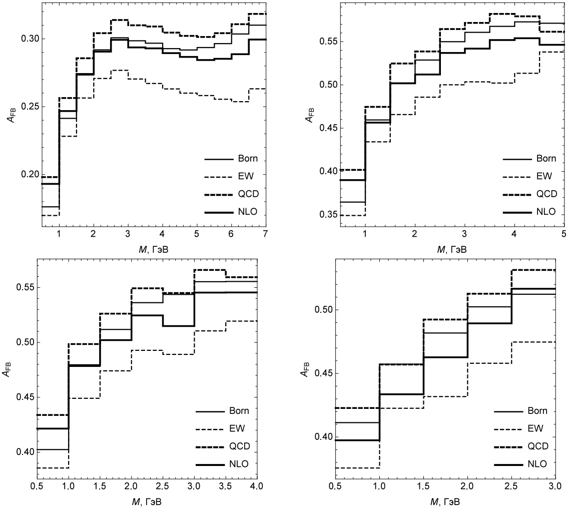

Figure 16: $A_{\rm FB}$ for $\mu^+\mu^-$-production: top – $|y| < 1$ and $1 < |y| < 1.25$, bottom – $1.25 < |y| < 1.5$ and $1.5 < |y| < 2.5$.

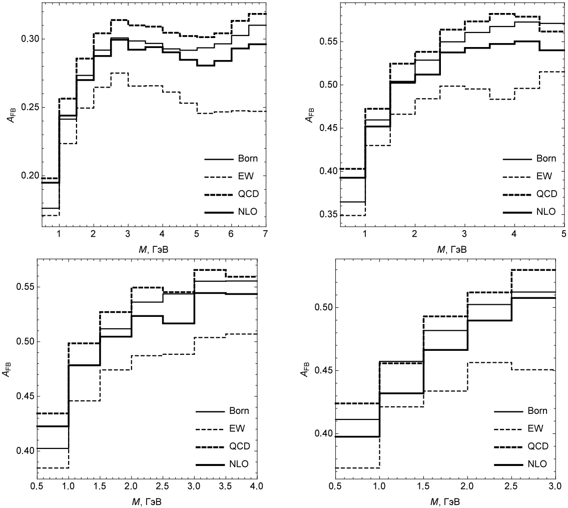

Figure 17: $A_{\rm FB}$ for e^+e^--production: top – $|y| < 1$ and $1 < |y| < 1.25$, bottom – $1.25 < |y| < 1.5$ and $1.5 < |y| < 2.5$.

A_{FB} for Run3 of CMS LHC: $\mu^+\mu^-$, DY and $\gamma\gamma$

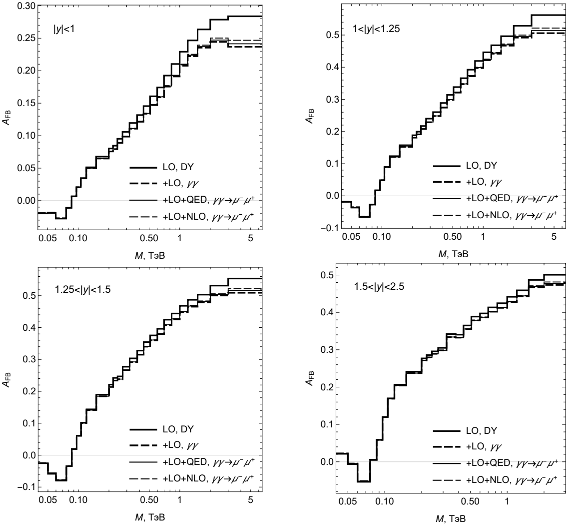

Figure 18: Forward-backward asymmetry A_{FB} for $\mu^+\mu^-$-production.

Conclusions & Acknowledgement

★ **The NLO EWK** corrections to dilepton production with Drell–Yan and $\gamma\gamma$-fusion mechanisms have been studied.

★ It has been ascertained that the considered in Run 3 region radiative corrections change the cross sections and A_{FB} **significantly**.

★ I would like to thank the **RDMS CMS group** members for the stimulating discussions and **CERN (CMS Group)** for warm hospitality during my visits.

★ This work was supported by the **Convergence-2025** Research Program of Republic of Belarus (Microscopic World and Universe Subprogram).

★ The numerical calcualtion was performed partically by **“HybriLIT”** Heterogeneous Platform of the Laboratory of Information Technologies of JINR.